Journal of
Materials Chemistry B

Materials for biology and medicine

Accepted Manuscript

This article can be cited before page numbers have been issued, to do this please use: L. Chen, Y. Zhang, N. Song, Y. Li, Z. Yang, T. Sun and Z. Xie, *J. Mater. Chem. B*, 2019, DOI: 10.1039/C9TB01165J.

This is an Accepted Manuscript, which has been through the Royal Society of Chemistry peer review process and has been accepted for publication.

Accepted Manuscripts are published online shortly after acceptance, before technical editing, formatting and proof reading. Using this free service, authors can make their results available to the community, in citable form, before we publish the edited article. We will replace this Accepted Manuscript with the edited and formatted Advance Article as soon as it is available.

You can find more information about Accepted Manuscripts in the Information for Authors.

Please note that technical editing may introduce minor changes to the text and/or graphics, which may alter content. The journal's standard Terms & Conditions and the Ethical guidelines still apply. In no event shall the Royal Society of Chemistry be held responsible for any errors or omissions in this Accepted Manuscript or any consequences arising from the use of any information it contains.

ROYAL SOCIETY OF CHEMISTRY

rsc.li/materials-b

View Article Online
DOI: 10.1039/C9TB01165J

ARTICLE

Received 00th January 20xx, Accepted 00th January 20xx

DOI: 10.1039/x0xx00000x

Comparison Study of Two Near-Infrared Coumarin-BODIPY Dyes for Bioimaging and Photothermal Therapy of Cancer

Yuandong Zhang,[a] Nan Song,[a] Yuanyuan Li,[c] Zhiyu Yang,[a] Li Chen,*[a] Tingting Sun, [b] Zhigang Xie*[b]

Near-infrared (NIR) responsive agents for cancer bioimaging and photothermal therapy are available and significant. Herein, we employed two easily available dyes, boron-dipyrromethane and coumarin, to synthesize a pair of coumarin-borondipyrromethane dyes with different conjugate degrees (BDC and BSC). The difference of conjugate degree made their photophysical properties poles apart. After self-assembling of BDC and BSC, the newly constructed nanoparticles (BDC NPs and BSC NPs) demonstrated good biocompatibility. Moreover, BDC NPs exhibited a good photothermal effect under irradiation of 808 nm laser which could effectively inhibit the growth of HeLa cells, and BSC NPs could quickly show a conspicuous fluorescence in the HeLa cells. The exploration demonstrates that the two organic dyes prepared with different conjugation degrees could provide new options for photothermal therapy of cancer and rapid bioimaging.

Introduction

Non-invasive treatment and bioimaging have attracted the researchers' interest. Photothermal therapy (PTT) is one of the emerging non-invasive treatment methods of cancer with low toxicity, high selectivity, and perfect biological adaptability[1-8]. Photothermal agents could convert the irradiated photon into heat, and the increasing temperature would induce the heat susceptive cancer cells apoptosis[9-12]. Near-infrared (NIR) light could penetrate deep tissues effectively, as a result, the absorption of photothermal agents in this interval is of great significance. Photothermal agents are commonly classified into inorganic nanomaterials such as gold nanomaterials[13-15] and metal-organic frameworks (MOFs)[16-19], and organic nanomaterials like porphyrin derivatives[20-22], cyanine dyes[23-25], and boron-dipyrromethenes (BODIPYs)[26-31]. Organic photothermal agents possess many advantages in terms of biocompatibility, metabolism, and potential biodegradability. Non-invasive bioimaging has been validated as a widely applicable tool for clinical diagnostics and laboratory studies[32, 33]. Today, a wide variety of bioimaging techniques such as ultrasound imaging (US)[34, 35], CT imaging[36, 37], magnetic resonance imaging (MRI)[38-40] and positron emission computed tomography (PET)[41, 42] and fluorescence imaging[43, 44] are deeply developed. Fluorescence imaging holds numbers of advantages such as nontoxicity, rapid feedback and high sensitivity. NIR fluorescence bioimaging agents with a strong competitive advantage are widely expanded in the fields of carbon dots[45-47], quantum dots[48], fluorescent proteins[49, 50], and organic dyes[51-55]. BODIPY and its derivatives have certain advantages, such as high molar extinction coefficient and photochemical stability[56, 57]. The core of BODIPY is easily modified, in particular, the 3,5positions are regularly employed to introduce the vinyl group which could broaden the conjugation degree of the molecule and cause the red shift of absorption wavelength to the NIR region. Coumarin, a common heterocyclic compound, owns an easily modified structure, as a result, it has a wide variety of derivatives and is always applied as bioluminescent probe[58-60].

Knoevenagel condensation reaction was typically a series of reactions which carbonyl compounds and the compounds with active methyl group under a base catalyzed condition were dehydrated to afford the α, β- unsaturated compounds. In synthesis of BODIPY derivatives, Knoevenagel condensation reaction was facilely and versatilely employed to efficiently tune BODIPY dyes for near-infrared absorption or emission[61-63].

Currently, the researchers usually use coumarin-BODIPY derivatives as sensitive fluorescent probes[64-67]. Nevertheless, the coumarin-BODIPY derivatives with near-infrared absorption and employed as a photothermal agent or a rapid fluorescence bioimaging agent have not been reported yet.

In this work, we synthesized two coumarin-BODIPY derivatives (BDC and BSC) by Knoevenagel condensation reaction with acetonitrile as solvent (Scheme 1). The difference between BDC and BSC is a 7-diethylaminocoumarin, which is linked to BODIPY by a π-π double bond. This dissimilarity has generated many differences between BDC and BSC in their photophysical properties, as well as their nanoparticles in photothermal effects, bioimaging, and photothermal toxicity. BSC possessed more excellent fluorescence performance, which laid a foundation for BSC NPs in bioimaging. BDC retained a longer absorption wavelength and a low fluorescence quantum

[a] Department of Chemistry, Northeast Normal University, 5268 Renmin Street, Changchun 130024, P. R. China. E-mail: chenl686@nenu.edu.cn.
[b] State Key Laboratory of Polymer Physics and Chemistry, Changchun Institute of Applied Chemistry, Chinese Academy of Sciences, 5625 Renmin Street, Changchun 130022, P. R. China. E-mail: xiez@ciac.ac.cn.
[c] The First Hospital of Jilin University, Xinmin Street, Changchun, Jilin 130021, P.R. China. E-mail: lyy2017@ciac.ac.cn.

Electronic Supplementary Information (ESI) available: [details of any supplementary information available should be included here]. See DOI: 10.1039/x0xx00000x

Journal Name
DOI: 10.1039/C9TB01165J

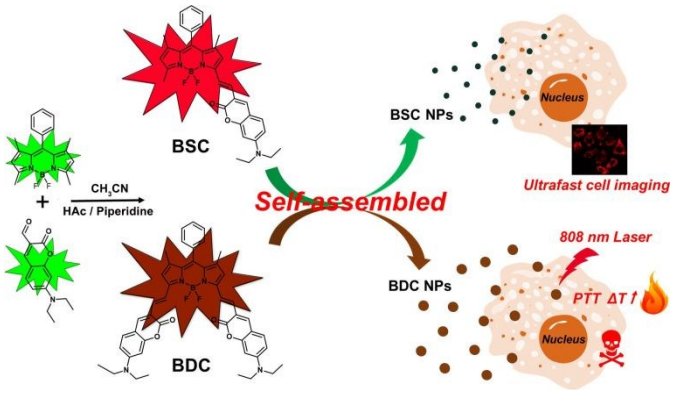

Scheme 1 Schematic illustration of BDC NPs and BSC NPs for their synthesis and different applications.

yield, which provided the precondition for BDC NPs to be applied in PTT tumor cells.

Experimental section

Synthesis of BDC and BSC

To increase the absorbance wavelength of BODIPY, we designed and synthesized the coumarin-BODIPY conjugate compounds. The synthesis routes of BDC and BSC were shown in Scheme 1, and the compounds 1 and 2 were detailed in Scheme S1, and S2 (ESI†). We confirmed BDC and BSC by ^{1}H NMR spectroscopy, ^{13}C NMR spectroscopy, and MS in Fig. S1 and S2 (ESI†).

BDC

Compound 1 (184 mg, 0.5 mM) and compound 2 (382 mg, 1.5 mM) were stirred in a solution of 30 mL acetonitrile, 1.0 mL piperidine and 0.8mL glacial acetic with a Dean-Stark apparatus at 90 °C for 8h under an argon atmosphere. Cooled, filtered, and washed with methanol then the solid was subjected to column chromatography through a silica gel column and eluted with DCM: EtOAc (100: 1) and finally dried in vacuum, a brown solid was afforded. Yield = 32% (124.5 mg, 0.16 mM); ^{1}H NMR (400 MHz, $CHCl_3$) δ 8.04 (s, 2H), 7.70 (d, J = 16.4 Hz, 2H), 7.49 - 7.46 (m, 4H), 7.43 (s, 1H), 7.39 (d, J = 9.2 Hz, 2H), 7.32 - 7.29 (m, 2H),
6.67 (s, 2H), 6.60 (dd, J = 8.8, 2.4 Hz, 2H), 6.48 (d, J = 2.4 Hz, 2H), 3.43 (q, J = 7.2 Hz, 8H), 1.41 (s, 6H), 1.22 (t, J = 7.0 Hz, 12H). ^{13}C NMR (500 MHz, $CHCl_3$) δ 161.81, 156.25, 152.42, 150.97, 141.97, 137.49, 133.76, 129.69, 129.54, 129.07, 128.97, 128.53, 118.48, 118.44, 117.02, 109.41, 109.39, 97.27, 44.99, 14.62,
12.56. MALDI-TOF/MS for $[BDC]^+$: 778.35 calcd, 778.4 found. **BSC**

As a by-product of BDC, BSC was present in the filtrate solution of BDC. Then collected and dried in vacuum, the mixture was subjected to column chromatography through a silica gel column and eluted with DCM, a deep green crystal was afforded. Yield = 8% (22 mg, 0.04 mM); ^{1}H NMR (400 MHz, $CHCl_3$) δ 7.99 (s, 1H), 7.62 (d, J = 16.6 Hz, 2H), 7.49 - 7.43 (m, 4H), 7.35 (d, J = 8.8 Hz, 2H), 7.30 - 7.27 (m, 4H), 6.65 (s, 1H), 6.60 (dd, J = 8.8, 2.4 Hz, 2H), 6.47 (d, J = 2.0 Hz, 1H), 5.99 (s, 1H), 3.41 (q, J = 7.2 Hz, 4H), 2.61 (s, 3H), 1.38 (d, J = 9.2 Hz, 6H), 1.22 (t, J = 7.2 Hz, 6H). ^{13}C NMR (500 MHz, $CHCl_3$) δ 161.87, 156.27, 154.90, 152.89, 151.00, 142.63, 140.10, 137.36, 135.08, 131.91, 129.66, 129.62, 129.11, 128.97, 128.22, 121.24, 118.28, 118.19, 116.87, 109.46, 109.27, 97.24, 44.97, 14.61, 14.37, 12.54.
MALDI-TOF/MS for $[BSC]^+$: 551.26 calcd, 551.3 found. **Preparation of BDC nanoparticles and BSC nanoparticles (BDC NPs and BSC NPs)**

By slowly adding, a 3 mL BDC-THF solution was dropped into a rapid stirring 10 ml water in 20 min. After addition, the mixed solution was further stirred at room temperature for another 16 hours, with the intention that THF in the mixture was diffused to the external environment, and the nanoparticles were uniformly and stably present in aqueous solution. With the same program, acetone was more suitable as a solvent for BSC to prepare a more concentrated BSC NPs solution. **Photothermal Activity and Photothermal Conversion Efficiency**

The BDC NPs and BSC NPs (65.0 μM, 200 μL) were under the irradiation of an 808 nm laser at the intensity of 0.70 W cm^{-2} for a period of 300 s with DI water as a control. To affirm the promising photothermal activity, we measured the different concentrations of BDC NPs were adopted and irradiated by an 808 nm laser (0.70 W cm^{-2}) for 300 s, and the 65.0 μM BDC NPs were under the irradiation of the 808 nm laser with different power densities for 300 s. The concentrations of BDC NPs we chose were 16.3 μM, 32.5 μM, 65.0 μM, the chose different power densities of 808 nm laser were 0.23 W cm^{-2}, 0.48 W cm^{-2} and 0.70 W cm^{-2}, the used amount of BDC NPs for each sample was 200 μL. The temperature recorder probe was hired to monitor the temperature changes and recorded 10 s a period. The 808 nm laser was in employment to irradiate the 70.0 μM BDC NPs until the temperature formed a plateau, then insulated the laser, recorded the whole temperature interval 10 s a count until the temperature restored to room temperature again. Then calculated photothermal conversion efficiency. The main text of the article should appear here with headings as appropriate.

Cell Imaging and Flow Cytometry

The HeLa cells were cultured in Dulbecco's Modified Eagle's Medium (DMEM; GIBCO) which composed by 10% fetal bovine serum (FBS) and 100X Penicillin/Streptomycin Solution under a mixed humidified atmosphere which 5% CO_2 contained at 37 °C. After a 12h culture, the HeLa cells were incubated with the nanoparticles (20.0 μM) for different time periods. Flow cytometry was hired with a flow cytometer by the method of cell imaging treatment process. **MTT assay**

The HeLa cells were planted at a density of 10^5 cells per well in 96-well plates then cultured in DMEM for 12 hours to allow cell adhesion. By engaging 200 μL of DMEM contained various concentrations BDC NPs instead of the medium, 6 hours later, a NIR 808 nm laser (0.70 W cm^{-2}) was hired to irradiate the cells for 5 min at 37 °C and culture for an additional 24 h. Then 20 μL MTT (5 mg mL^{-1}) assays were added to cells in each well and incubated for another 4 hours. Finally, removed the medium cleanly, and DMSO (150 μL) was added. The characteristic absorption at λ = 490 nm was determined and recorded by a microplate analyzer. **Live–Dead Cell Staining** To more directly demonstrate the efficiency of BDC NPs in photothermal toxicity for HeLa cells, calcein AM and

Journal Name ARTICLE
View Article Online
DOI: 10.1039/C9TB01165J

propidium iodide (PI) were employed to identify live (green) and dead (red) cells, respectively. The HeLa cells were treated with the same method in MTT assays, while the untreated cells as a control. The cells were incubated under a humidified 5% CO_2 contained mixed atmosphere at 37 °C for 24 h. Subsequently, the calceinAM/PI solution was employed to stain the cells for 40 min at room temperature. Finally, the cell staining results were acquired by a fluorescence microscope.

Cell apoptosis test

To investigate the anticancer mechanism of BDC NPs, flow cytometry experiments were performed to demonstrate the process of apoptosis, in this experiment 5×10^3 cells were collected for each sample. In 6-well plates, the HeLa cells were cultured in 1.5 mL medium for 12 h to obtain 3×10^5 cells per well. With the same method of live-dead cell staining, after a 24 h incubation discarded the medium in each well. The cells were washed by 1 mL PBS, then 0.5 mL trypsin was treated to disperse the cells. The harvested suspended cells were centrifuged at 2000 rpm for 5 min, discarded the supernatant and washed by PBS. Then repeated centrifugation and discarding, Annexin V-FITC and PI were employed to co-stain the cells in dark for 20 min. Finally, the cells were collected and evaluated by a flow cytometer.

Results and discussion

By employing UV-vis spectrophotometer and fluorescence spectrophotometer, the photophysical properties of BDC and BSC were recorded. BDC and BSC were synthesized from BODIPY and 7-diethylaminocoumarin via Knoevenagel condensation reaction. The newly generated π-π double bond and the one at the 3,4-position of 7-diethylaminocoumarin moiety formed conjugated double bonds, generated the conjugate effect, increased the degree of conjugation and caused red-shift of the maximum absorption wavelength. As exhibited in Fig. 1a, the, absorption spectrum of BDC in $CHCl_3$ disclosed two main peaks at 490 and 732 nm, as well as a weak hillock shape peak at 392 nm, while BSC owned two main peaks at 623 and 443 nm. In the fluorescence spectra, BDC and BSC possessed a 772 and 665 nm emission wavelength (Fig. 1b), and the relative fluorescence quantum yield (Φ_f) of BSC was 0.322, almost ten times higher than that of BDC (Φ_f = 0.037). The Stock shift (Δλ) of BDC and BSC was 40 and 42 nm, respectively. The photophysical data of BDC and BSC measured in $CHCl_3$ were presented in Table 1.

Both coumarin and BODIPY can achieve intramolecular charge transfer (ICT) by changing the substituents at different sites. In order to apprehend the charges transfer in BDC and BSC, we appointed the density functional theory (DFT) with B3LYP/6-31G(d) level of the Gaussian 09 program to calculate of the highest occupied molecular orbital (HOMO) and lowest unoccupied molecular orbital (LUMO) energy levels of BDC and BSC (Fig. 1c).

Table 1 Photophysical data of BDC and BSC (a) measured in $CHCl_3$, (b) measured for the nanoparticles of BDC and BSC in water.

Comp.	[a] λ_{max}, Abs (nm)	[a] λ_{max}, Em (nm)	[a] Δλ (nm)	[a] Φ_f	[b] λ_{max}, Abs (nm)
BDC	732	772	40	0.037	759
BSC	623	665	42	0.322	635

For BDC, we could unearth the charges distributed on HOMO and LUMO were different, and they had an apparent charge transfer tendency from the 7-diethylaminocoumarin moieties to the BODIPY core, which confirmed BDC possessed an ICT process. While the charge of BSC was regularly distributed on HOMO and LUMO, which indicated that the BSC molecule dominated a rarely ICT tendency.

Evidenced by transmission electron microscopy (TEM), the self-assembled BDC NPs and BSC NPs were confirmed as uniform solid spheres, and their sizes were about 160 and 100 nm respectively (Fig. 2a, S3 and S4). Dynamic light scattering (DLS) was usually used to support the results of TEM, the average hydrodynamic diameter and the polydispersity index (PDI) of BDC NPs were about 232 nm and 0.129 for each, and BSC NPs owned 197 nm and 0.134, respectively (Fig. S3 and S4). The stability in aqueous solution is one of the essential indicators for nanoparticles. In Fig. S3, BDC NPs and BSC NPs were given eight days tested of hydrodynamic diameter and PDI in aqueous solution, and they did not exhibit a significant amplitude.

After characterizing the morphology of BDC NPs and BSC NPs, we determined their absorption spectra (Fig. 2b). Compared with the absorption spectra of their respective molecules in chloroform, the absorption peak shape of nanoparticles was

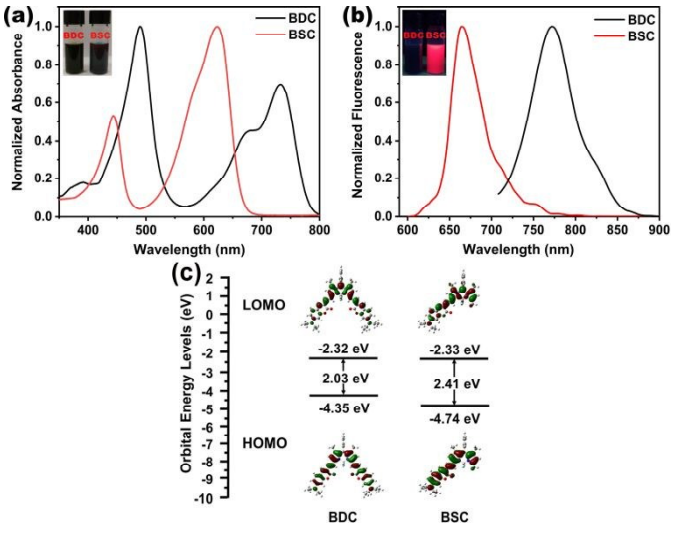

Fig. 1 The normalized absorption spectra (a) and fluorescence spectra (b) of BDC and BSC in $CHCl_3$ with the built-in images of BDC and BSC in $CHCl_3$ under daylight (a) and upon excitation by 365 nm lamp (b). (c) Electron density contours and orbital energies calculated for the HOMO and LUMO of BDC and BSC at the Beck3LYP/DZP level in vacuum.

View Article Online
DOI: 10.1039/C9TB01165J

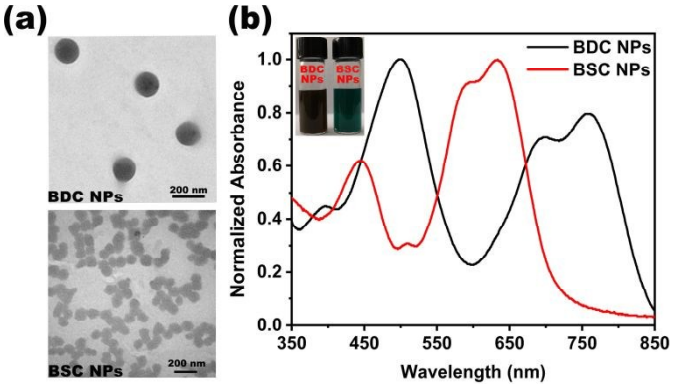

Fig. 2 The Basic physical properties of BDC NPs and BSC NPs. (a) The TEM images of BDC NPs and BSC NPs. (b) The normalized absorbance spectra of BDC NPs and BSC NPs.

basically the same. However, the maximum absorption wavelengths of BDC NPs and BSC NPs had a specific red shift than the molecular ones. The λ_{max} of BDC NPs was 759 nm, a 27 nm red shift than BDC in chloroform, in contrast, the red shift degree of BSC NPs was much lower as a 12 nm red shift (635 nm). The longer maximum absorption wavelength of BDC NPs forecasted a higher absorption intensity in the near-infrared region.

To investigate the photothermal properties of BDC NPs and BSC NPs, firstly, we recorded and compared the photothermal heating curves of 65.0 μM BDC NPs, BSC NPs and water with an 808 nm laser (0.70 W cm^{-2}) irradiation for 300 s (Fig. 3a). Only BDC NPs were prompted a remarkable temperature change (ΔT: 35.6 °C), while BSC NPs and water had little temperature changes, which might be determined by whether the absorption wavelength located at 808 nm. Then the photothermal performance of BDC NPs with different laser power intensities and concentrations was tested. In Fig. 3b and 3c, we investigated the heating effect of BDC NPs under 808 nm laser irradiation for 300 s and the result showed that the heating effect was not only laser-power intensity dependent but also concentration dependent. To measure the photothermal conversion efficiency of BDC NPs, a 300 s heating curve was collected from the nanoparticles (70.0 μM) under 808 nm laser irradiation at a power density of 0.70 W cm^{-2} (Fig. 3d). Then we removed the irradiation and recorded a cooling time plot versus negative natural logarithm of the temperature as revealed in Fig. 3e (τ= 183 s) to evaluate the photothermal conversion efficiency (η), and the calculated value was 25%. After five cycles of heating and cooling, BDC NPs still had an apparent photothermal effect, which represented good photothermal stability.

The cellular uptake for BDC NPs and BSC NPs was explored by confocal laser scanning microscopy (CLSM). HeLa cells were incubated with BDC NPs and BSC NPs with different time at 37 °C. As revealed in Fig. 4a and 5a, the green and red fluorescence were found in the cytoplasm around the nuclei of the cells under 488 nm (green channel) and 555 nm (red channel) laser

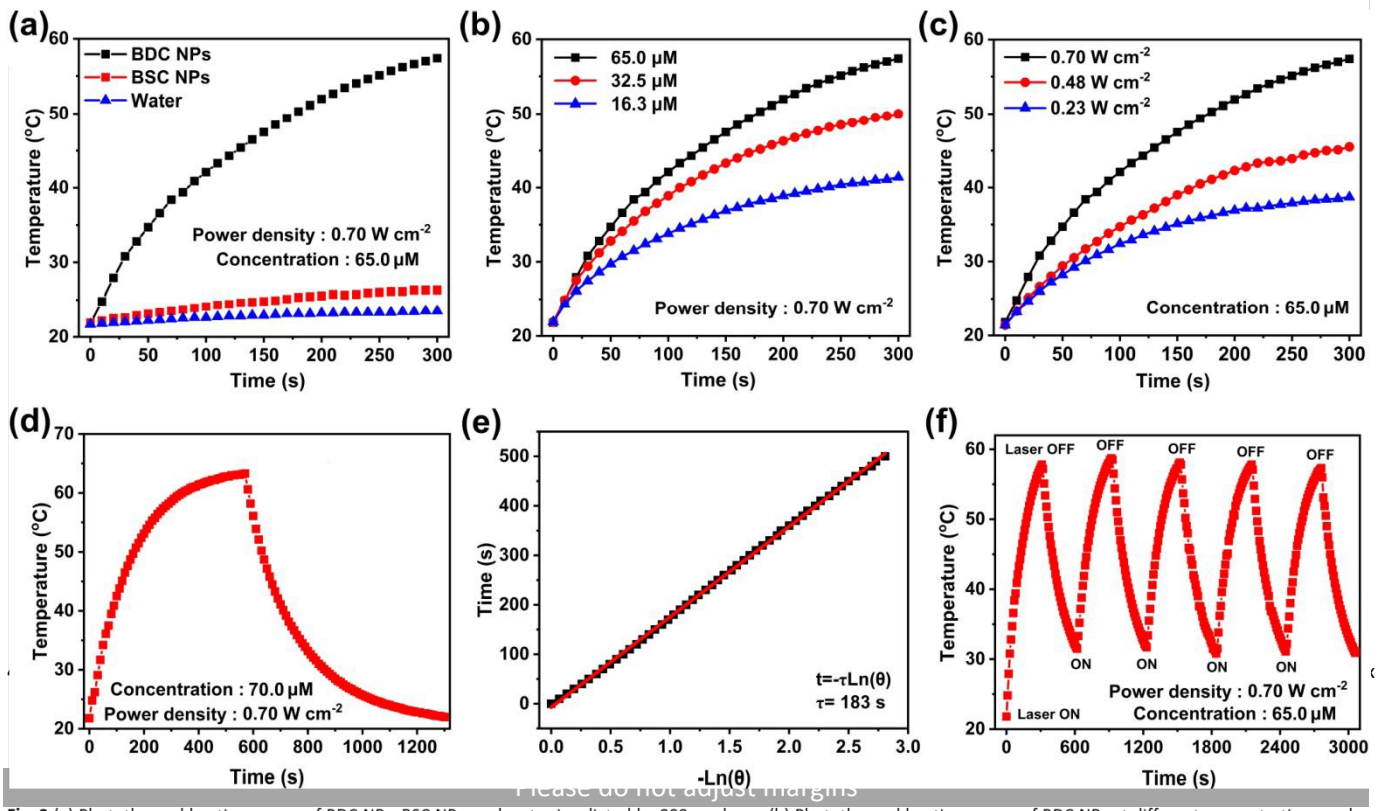

Fig. 3 (a) Photothermal heating curves of BDC NPs, BSC NPs, and water irradiated by 808 nm laser. (b) Photothermal heating curves of BDC NPs at different concentrations under 808 nm laser irradiation. (c) Photothermal heating curves of 65.0 μM BDC NPs under 808 nm laser irradiation with different laser power densities. (d) The photothermal response of BDC NPs irradiated by the 808 nm laser for 300 s subsequently got rid of the laser. (e) Plot of cooling time versus negative natural logarithm of the temperature obtained from the cooling stage of (d). (f) The temperature records of BDC NPs under laser irradiation (0.70 W cm^{-2}) for five times with the laser being turned on/off by 300 s a cycle.

View Article Online
DOI: 10.1039/C9TB01165J

excitation after the incubation with BDC NPs and BSC NPs, which confirmed BDC NPs and BSC NPs could be gradually endocytosed and enriched in the cytoplasm. By comparing with the fluorescence intensities under red channel laser excitation in different time periods, a clear tendency of enhancement could be observed from the cells incubated with BDC NPs from 1 to 6 h, signifying that the BDC NPs could be continuous internalized by HeLa cells (Fig. 4b and 4c). Surprisingly, with the same concentration of BDC NPs, BSC NPs only needed 1 minute incubation with the HeLa cells to show a similar fluorescence intensity as BDC NPs incubated with the cells for 6 hours (Fig. 4b, 4c, 5b and 5c). This phenomenon meant BSC NPs could quickly stain the HeLa cells in a very short time (1 minute). With the incubation time of BSC NPs going to 10 minutes, the fluorescence intensity in HeLa cells was times higher than the incubation of 1 minute (Fig. 5b and 5c). It probably because BSC NPs owned a small size and superior photophysical properties. With the same conditions, the flow cytometry results could also demonstrate that both BDC NPs and BSC NPs could have a tendency to accumulate in HeLa cells (Fig. 4d and 5d). The consequences established that BSC NPs could not only be

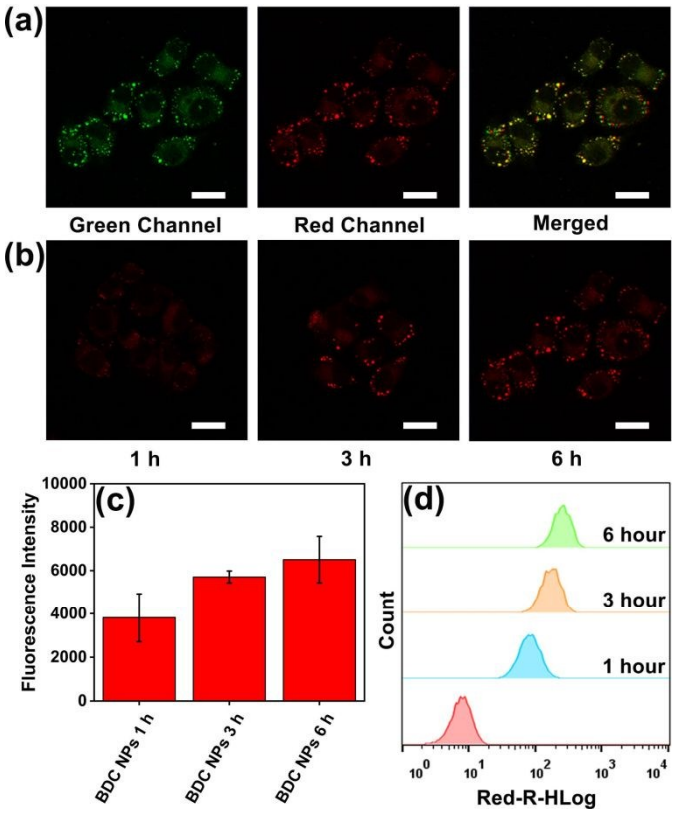

Fig. 4 The CLSM images of (a) HeLa cells incubated with BDC NPs (20.0 μM) for 6 h under the excitation of different channels, Scale bars: 20 μm. (b) HeLa cells incubated with BDC (20.0 μM) for different periods in the red channel, Scale bars: 20 μm. (c) Relative fluorescence intensity of HeLa cells incubated with BDC NPs under the same condition as the CLSM images for different periods in the red channel. (d) The flow cytometry analysis of the HeLa cells incubated with BDC NPs under the same condition as the CLSM images for different periods by flow cytometry.

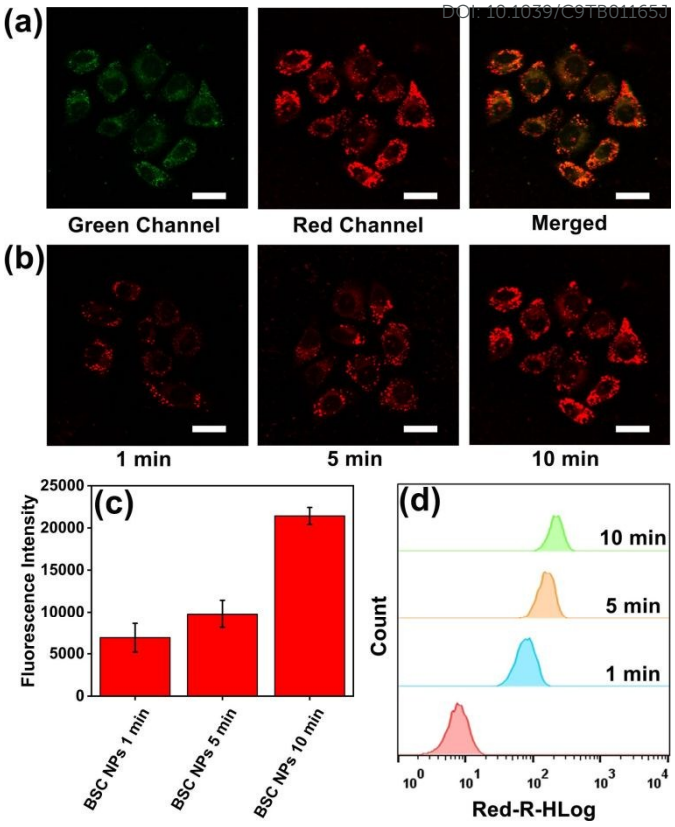

Fig. 5 The CLSM images of (a) HeLa cells incubated with BSC (20.0 μM) for 10 min under the excitation of different channels, Scale bars: 20 μm. (b) HeLa cells incubated with BSC (20.0 μM) for different periods in the red channel, Scale bars: 20 μm. (c) Relative fluorescence intensity of HeLa cells incubated with BSC NPs under the same condition as the CLSM images for different periods in the red channel. (d) The flow cytometry analysis of the HeLa cells incubated with BSC NPs under the same condition of the CLSM images for different periods with control of untreated cells by flow cytometry.

internalized by cells in a very short time but also be supported as a rapid cell imaging agent.

To appraise the phototherapy efficacy of BDC NPs for cancer and the biocompatibility of BSC NPs for bioimaging, the cytotoxicity of BDC NPs and BSC NPs toward HeLa and L929 cells were measured by 3-(4,5-dimethylthiazol-2-yl)-2,5-diphenyltetrazolium bromide (MTT) assays. No cytotoxicity was observed from HeLa and L929 cells incubated with BDC NPs and BSC NPs in the dark (Fig. 6a and S5), which demonstrated that BDC NPs and BSC NPs were biocompatible. Compared with the biocompatibility in dark, BDC NPs possessed a concentration dependent cytotoxicity toward HeLa and L929 cells under 808 nm laser irradiation (0.70 W cm^{-2}, 5 min). The concentration of 26.0 μM BDC NPs was sufficient to eradicate the vast majority of the co-incubated HeLa cells under the irradiation. By calculation, a half maximal inhibitory concentration (IC_{50}) value of BDC NPs was 14.4 μM. Such good biocompatibility and superior phototoxicity proved BDC NPs had great potential as a photothermal agent to be applied in the field of cancer photothermal clinical treatment.

To intuitively define the phototoxicity of BDC NPs toward the HeLa cells, the live-dead cell staining experiment was established. For

DOI: 10.1039/C9TB01165J

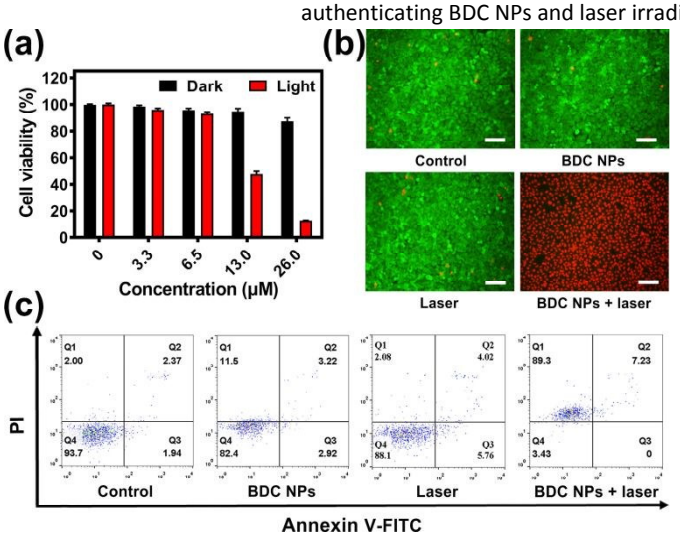

Fig. 6 Cytotoxicity against HeLa cells. (a) The viability of the cells exposed under the irradiation of 808 nm laser (0.70 W cm $^{-2}$) for 5 min. (b) The live (green) and dead (red) fluorescence images of the cells co-stained with calcein-AM and PI after different treatments, Scale bars: 100 μm. (c) The flow cytometry apoptosis analysis of the HeLa cells treated with different conditions; the four regions represent different stages, Q1: cell necrosis, Q2: late apoptosis, Q3: early apoptosis, and Q4: survival.

and propidium iodide (PI) were imposed on making a distinction between the living cells with green fluorescence and the dead ones with red fluorescence (Fig. 6b). The cells treated with laser irradiation or BDC NPs in dark could maintain the normal morphology, which indicated they were as healthy as the ones in the control group with apparent green fluorescence. Contrariwise, the cells incubated with BDC NPs and irradiated with laser were demonstrated a garish red fluorescence, and the cell morphology was irreversibly destroyed.

To ascertain the evolution of the cell death, flow cytometry apoptosis analysis was taken advantage to clarify the approach which BDC NPs and the 808 nm laser involved in cancer treatment. The fluoresceine isothiocyanate (Annexin V-FITC) and PI were utilized in double-labeled HeLa cells to single out the process of the cells such as early apoptotic cells, late apoptotic cells, necrotic cells, and live cells. In Fig. 6c, a safe rate of cell apoptosis (Q1+Q2+Q3) exhibited in the control group, the cells incubated with BDC NPs group and the cells under 808 nm laser irradiation group. The group of the cells treated with BDC NPs and laser irradiation demonstrated a perfect necrotic cell rate (Q1) of 89.3%, which explained the collaboration of BDC NPs and laser irradiation produced heat and caused the necrosis of cells. As expected, the flow cytometry analysis results were practically consistent with the MTT consequences and validated that the progress of BDC NPs and laser irradiation anticancer was achieved by photothermal toxicity caused cell necrosis.

Conclusions

In summary, we designed and synthesized a pair of novel nearinfrared coumarin-BODIPY dyes, which could self-assemble into organic nanoparticles. BDC and BSC presented different conjugation degree, absorption wavelength, and fluorescence characteristics. The differences between BDC and BSC were expanded on their authenticating BDC NPs and laser irradiation was the triggering of the cell death, calcein-acetoxymethyl (AM) nanoparticles. BDC NPs and BSC NPs exhibited a good biocompatibility in dark. BDC NPs demonstrated the phototoxicity by the irradiation of 808 nm laser toward the HeLa cells and BSC NPs could be employed as a rapid cell imaging agent. Consequently, we can assert that BDC NPs could be applied as a photothermal agent in cancer treatment and BSC NPs could be a rapid bioimaging agent.

Conflicts of interest

There are no conflicts to declare.

Acknowledgements

This work was supported by the National Natural Science Foundation of China (Project No. 21474012, 51273037).

Notes and references

1. Y. Jiang, J. Li, X. Zhen, C. Xie and K. Pu, *Adv. Mater.*, 2018, **30**, 1705980.
2. H. S. Jung, P. Verwilst, A. Sharma, J. Shin, J. L. Sessler and J. S. Kim, *Chem. Soc. Rev.*, 2018, **47**, 2280-2297.
3. X. Li, H. Bai, Y. Yang, J. Yoon, S. Wang and X. Zhang, *Adv. Mater.*, 2019, **31**, 1805092.
4. Y. Liu, P. Bhattarai, Z. Dai and X. Chen, *Chem. Soc. Rev.*, 2019, **48**, 2053-2108.
5. L. Y. Zhao, Y. M. Liu, R. Chang, R. R. Xing and X. H. Yan, *Adv. Funct. Mater.*, 2019, **29**, 1806877.
6. H. S. Jung, J. H. Lee, K. Kim, S. Koo, P. Verwilst, J. L. Sessler, C. Kang and J. S. Kim, *J. Am. Chem. Soc.*, 2017, **139**, 9972-9978.
7. N. Shao, Y. Qi, H. Lu, D. He, B. Li and Y. Huang, *ACS Biomater. Sci. Eng.*, 2018, **5**, 795-804.
8. Y. Yan, J. Chen, Z. Yang, X. Zhang, Z. Liu and J. Hua, *J. Mater. Chem. B*, 2018, **6**, 7420-7426.
9. Y. Cai, W. Si, W. Huang, P. Chen, J. Shao and X. Dong, *Small*, 2018, **14**, 1704247.
10. Y. Lyu, J. Zeng, Y. Jiang, X. Zhen, T. Wang, S. Qiu, X. Lou, M. Gao and K. Pu, *ACS Nano*, 2018, **12**, 1801-1810.
11. J. Nam, S. Son, L. J. Ochyl, R. Kuai, A. Schwendeman and J. J. Moon, *Nat. Commun.*, 2018, **9**, 1074.
12. H. Wang, J. Chang, M. Shi, W. Pan, N. Li and B. Tang, *Angew. Chem. Int. Ed. Engl.*, 2019, **58**, 1057-1061.
13. Z. D. Hood, K. P. Kubelick, K. D. Gilroy, D. Vanderlaan, X. Yang, M. Yang, M. Chi, S. Y. Emelianov and Y. Xia, *Nanoscale*, 2019, **11**, 3013-3020.
14. N. Khlebtsov and L. Dykman, *Chem. Soc. Rev.*, 2011, **40**, 1647-1671.
15. L. Dykman and N. Khlebtsov, *Chem. Soc. Rev.*, 2012, **41**, 2256-2282.
16. W. Zhu, Y. Liu, Z. Yang, L. Zhang, L. J. Xiao, P. Liu, J. Wang, C. F. Yi, Z. S. Xu and J. H. Ren, *J. Mater. Chem. B*, 2018, **6**, 265-276.

View Article Online
DOI: 10.1039/C9TB01165J

17. X. H. Zheng, L. Wang, M. Liu, P. P. Lei, F. Liu and Z. G. Xie, *Chem. Mater.*, 2018, **30**, 6867-6876.
18. Y. Li, N. Xu, J. Zhou, W. Zhu, L. Li, M. Dong, H. Yu, L. Wang, W. Liu and Z. Xie, *Biomater. Sci.*, 2018, **6**, 2918-2924.
19. J. Feng, Z. Xu, P. Dong, W. Q. Yu, F. Liu, Q. Y. Jiang, F. Wang and X. Q. Liu, *J. Mater. Chem. B*, 2019, **7**, 994-1004.
20. X. H. Zheng, L. Wang, S. Liu, W. Zhang, F. G. Liu and Z. G. Xie, *Adv. Funct. Mater.*, 2018, **28**, 1706507.
21. R. Xing, Q. Zou, C. Yuan, L. Zhao, R. Chang and X. Yan, *Adv. Mater.*, 2019, DOI: 10.1002/adma.201900822, 1900822.
22. X. Li, C. Y. Kim, S. Lee, D. Lee, H. M. Chung, G. Kim, S. H. Heo, C. Kim, K. S. Hong and J. Yoon, *J. Am. Chem. Soc.*, 2017, **139**, 10880-10886.
23. Y. Deng, L. Huang, H. Yang, H. Ke, H. He, Z. Guo, T. Yang, A. Zhu, H. Wu and H. Chen, *Small*, 2017, **13**, 1602747.
24. J. X. Zhang, S. Liu, X. L. Hu, Z. G. Xie and X. B. Jing, *ACS Biomater. Sci. Eng.*, 2016, **2**, 1942-1950.
25. C. Gao, X. Liang, S. Mo, N. Zhang, D. Sun and Z. Dai, *ACS Appl. Mater. Interfaces*, 2018, **10**, 3219-3228.
26. N. Song, L. Fu, Y. Liu, Y. Y. Li, L. Chen, X. Y. Wang, S. Liu and Z. G. Xie, *Dyes Pigm.*, 2019, **162**, 295-302.
27. X. Wang, W. Lin, W. Zhang, C. Li, T. Sun, G. Chen and Z. Xie, *J. Colloid Interface Sci.*, 2019, **536**, 208-214.
28. W. Sun, X. Zhao, J. Fan, J. Du and X. Peng, *Small*, 2019, DOI: 10.1002/smll.201804927, 1804927.
29. X. Chen, Q. Wang, L. Liu, T. Sun, W. Zhou, Q. Chen, Y. Lu, X. He, Y. Zhang, Y. Zhang, C. Ruan, Q. Guo, C. Li and C. Jiang, *Biomaterials*, 2018, **183**, 258-267.
30. D. Chen, J. Zhang, Y. Tang, X. Huang, J. Shao, W. Si, J. Ji, Q. Zhang, W. Huang and X. Dong, *J. Mater. Chem. B*, 2018, **6**, 4522-4530.
31. D. Chen, Q. Tang, J. Zou, X. Yang, W. Huang, Q. Zhang, J. Shao and X. Dong, *Adv. Healthcare Mater.*, 2018, **7**, 1701272.
32. Y. Wang, K. Zhou, G. Huang, C. Hensley, X. Huang, X. Ma, T. Zhao, B. D. Sumer, R. J. DeBerardinis and J. Gao, *Nat. Mater.*, 2014, **13**, 204-212.
33. D. E. Lee, H. Koo, I. C. Sun, J. H. Ryu, K. Kim and I. C. Kwon, *Chem. Soc. Rev.*, 2012, **41**, 2656-2672.
34. W. Tang, Z. Yang, S. Wang, Z. Wang, J. Song, G. Yu, W. Fan, Y. Dai, J. Wang, L. Shan, G. Niu, Q. Fan and X. Chen, *ACS Nano*, 2018, **12**, 2610-2622.
35. Y. Wang, G. Sui, D. Teng, Q. Wang, J. Qu, L. Zhu, H. Ran, Z. Wang, C. Jin and H. Wang, *Biomater. Sci.*, 2018, **7**, 196-210.
36. H. Zhang, Q. Zhang, C. Liu and B. Han, *Biomater. Sci.*, 2019, **7**, 1696-1704.
37. D. L. Kraitchman, M. Tatsumi, W. D. Gilson, T. Ishimori, D. Kedziorek, P. Walczak, W. P. Segars, H. H. Chen, D. Fritzges, I. Izbudak, R. G. Young, M. Marcelino, M. F. Pittenger, M. Solaiyappan, R. C. Boston, B. M. Tsui, R. L. Wahl and J. W. Bulte, *Circulation*, 2005, **112**, 1451-1461.
38. P. Vemuri, T. G. Lesnick, S. A. Przybelski, J. Graff-Radford, R. I. Reid, V. J. Lowe, S. M. Zuk, M. L. Senjem, C. G. Schwarz, J. L. Gunter, K. Kantarci, M. M. Machulda, M. M. Mielke, R. C. Petersen, D. S. Knopman and C. R. Jack, Jr., *Ann. Neurol.*, 2018, **84**, 705-716.
39. F. Liu, X. Li, Y. Li, Y. Qi, H. Yuan, J. He, W. Li and M. Zhou, *Biomater. Sci.,* 2019, DOI: 10.1039/c9bm00056a.
40. G. Bell, G. Balasundaram, A. B. E. Attia, F. Mandino, M. Olivo and I. P. Parkin, *J. Mater. Chem. B*, 2019, **7**, 2212-2219.
41. N. Adonai, N. Adonai, K. N. Nguyen, J. Walsh, M. Iyer, T. Toyokuni, M. E. Phelps, T. McCarthy, D. W. McCarthy and S. S. Gambhir, *Proc. Natl. Acad. Sci. U. S. A.*, 2002, **99**, 3030-3035.
42. Y. Sun, X. Zeng, Y. Xiao, C. Liu, H. Zhu, H. Zhou, Z. Chen, F. Xu, J. Wang, M. Zhu, J. Wu, M. Tian, H. Zhang, Z. Deng, Z. Cheng and X. Hong, *Chem. Sci.*, 2018, **9**, 2092-2097.
43. Z. Guo, S. Park, J. Yoon and I. Shin, *Chem. Soc. Rev.*, 2014, **43**, 16-29.
44. G. Hong, A. L. Antaris and H. Dai, *Nat. Biomed. Eng.*, 2017, **1**, 0010.
45. H. He, X. Zheng, S. Liu, M. Zheng, Z. Xie, Y. Wang, M. Yu and X. Shuai, *Nanoscale*, 2018, **10**, 10991-10998.
46. L. Qiao, T. Sun, X. Zheng, M. Zheng and Z. Xie, *Mater. Sci. Eng. C Mater. Biol. Appl.*, 2018, **85**, 1-6.
47. M. Zheng, S. Ruan, S. Liu, T. Sun, D. Qu, H. Zhao, Z. Xie, H. Gao, X. Jing and Z. Sun, *ACS Nano*, 2015, **9**, 11455-11461.
48. J. Zhang, J. Qian, Q. Mei, L. Yang, L. He, S. Liu, C. Zhang and K. Zhang, *Biosens. Bioelectron.*, 2019, **128**, 61-67.
49. Y. Liu, C. H. Wolstenholme, G. C. Carter, H. Liu, H. Hu, L. S. Grainger, K. Miao, M. Fares, C. A. Hoelzel, H. P. Yennawar, G. Ning, M. Du, L. Bai, X. Li and X. Zhang, *J. Am. Chem. Soc.*, 2018, **140**, 7381-7384.
50. N. Coquelle, M. Sliwa, J. Woodhouse, G. Schiro, V. Adam, A. Aquila, T. R. M. Barends, S. Boutet, M. Byrdin, S. Carbajo, E. De la Mora, R. B. Doak, M. Feliks, F. Fieschi, L. Foucar, V. Guillon, M. Hilpert, M. S. Hunter, S. Jakobs, J. E. Koglin, G. Kovacsova, T. J. Lane, B. Levy, M. Liang, K. Nass, J. Ridard, J. S. Robinson, C. M. Roome, C. Ruckebusch, M. Seaberg, M. Thepaut, M. Cammarata, I. Demachy, M. Field, R. L. Shoeman, D. Bourgeois, J. P. Colletier, I. Schlichting and M. Weik, *Nat. Chem.*, 2018, **10**, 31-37.
51. X. Yang, N. N. Shi, L. Bai, Y. Ni, J. W. Li, W. L. Si, L. Li, J. J. Shao, W. Huang and X. C. Dong, *Dyes Pigm.*, 2018, **157**, 396-404.
52. H. Wan, J. Yue, S. Zhu, T. Uno, X. Zhang, Q. Yang, K. Yu, G. Hong, J. Wang, L. Li, Z. Ma, H. Gao, Y. Zhong, J. Su, A. L. Antaris, Y. Xia, J. Luo, Y. Liang and H. Dai, *Nat. Commun.*, 2018, **9**, 1171.
53. Q. Miao and K. Pu, *Adv. Mater.*, 2018, **30**, 1801778.
54. B. Li, L. Lu, M. Zhao, Z. Lei and F. Zhang, *Angew. Chem. Int. Ed. Engl.*, 2018, **57**, 7483-7487.
55. W. Fan, H. Deng, L. Zhu, C. Tu, Y. Su, L. Shi, J. Yang, L. Zhou, L. Xu and X. Zhu, *Biomater. Sci.*, 2019, DOI: 10.1039/c9bm00255c.
56. A. Turksoy, D. Yildiz and E. U. Akkaya, *Coord. Chem. Rev.*, 2019, **379**, 47-64.
57. J. Zou, P. Wang, Y. Wang, G. Liu, Y. Zhang, Q. Zhang, J. Shao, W. Si, W. Huang and X. Dong, *Chem. Sci.*, 2019, **10**, 268-276.
58. D. K. Sharma, S. T. Adams, Jr., K. L. Liebmann, A. Choi and S. C. Miller, *Org. Lett.*, 2019, **21**, 1641-1644.
59. Y. Bian, Z. Wei, Z. Wang, Z. Tu, L. Zheng, W. Wang, X. Leng and Y. Li, *J. Mater. Chem. B*, 2019, **7**, 2261-2276.
60. S. Feng, D. Liu and G. Feng, *Anal. Chim. Acta*, 2019, **1054**, 137-144.
61. X. Xia, Y. Qian and B. Shen, *J. Mater. Chem. B*, 2018, **6**, 30233029.
62. M. H. Chua, T. Kim, Z. L. Lim, T. Y. Gopalakrishna, Y. Ni, J. Xu, D. Kim and J. Wu, *Chem. Eur. J.*, 2018, **24**, 2232-2241.

View Article Online
DOI: 10.1039/C9TB01165J

63. S. Zhu, J. Zhang, G. K. Vegesna, R. Pandey, F.-T. Luo, S. A. Green and H. Liu, *Chem. Commun.*, 2011, **47**, 3508-3510.
64. K. B. Zheng, H. Chen, S. R. Fang and Y. Wang, *Sens. Actuators, B*, 2016, **233**, 193-198.
65. Y. Qian, B. Yang, Y. Shen, Q. Du, L. Lin, J. Lin, H. J. S. Zhu and A. B. Chemical, *Sensors Actuators B: Chem.*, 2013, **182**, 498-503.
66. H. Lee, Z. Yang, Y. Wi, T. W. Kim, P. Verwilst, Y. H. Lee, G. I. Han, C. Kang and J. S. Kim, *Bioconjugate Chem.*, 2015, **26**, 2474-2480.
67. X. Cao, W. Lin, Q. Yu and J. Wang, *Org. Lett.*, 2011, **13**, 60986101.

View Article Online
DOI: 10.1039/C9TB01165J

Graphic Abstract

Herein, two novel NIR Coumarin BODIPYs with different conjugation degrees were comparatively investigated for photothermal therapy and fluorescent bioimaging.